Energy 246 (2022) 123416

Contents lists available at ScienceDirect

Energy

journal homepage: www.elsevier.com/locate/energy

Experimental study on energy storage performances of packed bed with different solid materials

Hao Zhou*, Zhenya Lai, Kefa Cen

State Key Laboratory of Clean Energy Utilization, Institute for Thermal Power Engineering, Zhejiang University, Hangzhou, 310027, China

ARTICLE INFO

Article history:
Received 8 August 2021
Received in revised form
23 December 2021
Accepted 5 February 2022
Available online 9 February 2022

Keywords:
Thermal energy storage
Packed bed
Thermal performance
Storage materials
Thermocline characteristics

ABSTRACT

The physical properties of the solid materials as energy storage mediums are one of the main parameters that affect the design of the packed bed. Different solar applications may require different heating rates and temperatures, so choosing appropriate storage materials is essential. This paper compares the applicability of sintered ore particles, aluminium oxide balls, and rock crushed as sensible heat storage materials. The results show that the volumetric heat capacity of the sinter at 200 °C is 3253.7 kJ/(m^3·K), which is between aluminium oxide and rock. Rock is only suitable for heat storage below 550 °C, while sinter is the best candidate material for storing heat at ultra-high temperatures as high as 1000 °C. Moreover, the energy storage tests of packed beds using three materials under different operating conditions were also carried out. The results show that the heat capacity and voidage of the bed are the most critical factors affecting the thermal behavior of the bed, while the thermal conductivity of the material has a minor effect. After the system is stable, the energy recovery efficiency of the rock, aluminium oxide and sinter bed can reach 73.7%, 69.3%, and 66.8%, respectively, at a flow rate of 175 m^3/h.

1. Introduction

To achieve sustainable development, the shortage of traditional energy sources and the pressure of environmental pollution have forced worldwide scholars to shift their research focus to renewable energy [1]. The sun is a huge energy source, and only a tiny part of the solar energy reaching the earth is enough to meet human needs. However, discontinuity and instability are the biggest obstacles to the application of solar energy [2]. To use solar energy uninterruptedly, a thermal energy storage (TES) system that can compensate the mismatch between solar energy generation and demand is necessary [3].

Current liquid-phase energy storage systems such as water/steam and molten salt face high costs and limited operating temperatures [4]. The packed bed sensible heat storage system can use air as the heat transfer fluid and use cheap materials such as rocks as storage materials. Meanwhile, it can be equipped with a single-tank thermocline system, which has a significant cost advantage. Furthermore, if using air as the heat transfer fluid, the storage temperature can be unlimited [5], which can not only meet the needs of ultra-high temperature power cycles but also meet the low-temperature production needs of industrial workshops such as food, textile and paper plants [6].

The physical properties of solid materials as storage mediums are one of the main factors affecting the design of packed beds [7]. Different solar energy applications may require different heating rates and temperatures, so choosing suitable storage materials is significant. Moreover, it is necessary to comprehensively understand the effect of material properties on the thermal behavior of the packed bed. In this field, Gautam et al. [8] reviewed and compared various storage materials. In terms of characterization, Brosseau et al. [9] evaluated the performance of quartzite and silica sand in a 500 °C molten salt environment, and the results showed that both are suitable storage materials for parabolic trough power plants. Allen et al. [10] studied the applicability of different rocks as storage materials through literature review and thermal cycle testing. High-grade igneous rocks and metamorphic rocks are considered suitable. Hrifech et al. [11] used various characterization methods to evaluate the applicability of four natural rocks as medium-temperature (100–300 °C) storage materials and explained the correlation between petrological properties and thermophysical properties. The results show that all the rocks

* Corresponding author.
E-mail address: zhouhao@zju.edu.cn (H. Zhou).

https://doi.org/10.1016/j.energy.2022.123416
0360-5442/

Nomenclature

A	internal cross-sectional area of the tank, m^2
c_{pair}	specific heat capacity of air, J/(kg K)
E_{input}	input energy, J
E_{pump}	pumping work, J
H	bed height, mm
I	number of storage material layers
i	storage material layer
k	absolute permeability, m^2
m	air mass flow, kg/s
$Q_{release}$	instantaneous amount of energy released from the packed bed, J
Q_{stored}	instantaneous amount of energy stored in the packed bed, J
Str	stratification number
Str^*	Str number after normalization
T_{in}	air temperature at the inlet of the tank, °C
T_{ini}	initial temperature of the bed at t = 0, °C
T_{out}	air temperature at the outlet of the tank, °C
U	air superficial velocity in the tank, m/s
u	dynamic viscosity of the flowing fluid, Pa*s
V	air flow, m^3/h
x	radial position inside the tank, mm
y	axial position inside the tank, mm

Greek symbols

Δp	pressure drop over the tank, Pa
Δy	distance between temperature sensors, mm
ε	voidage of packed bed
$\eta_{charging}$	charging efficiency
$\eta_{discharging}$	discharging efficiency
η_{cycle}	overall cycle efficiency
ρ_{air}	air density, kg/m^3
ρ_a	apparent density of the storage material, kg/m^3
ρ_b	bulk density of the storage material, kg/m^3

studied are potential candidates. In terms of numerical simulation, Calderon-Vasquez et al. [12] evaluated the potential of copper slag as a storage material. Compared with other materials, copper slag has a steeper thermocline and higher energy stored due to higher heat capacity. Ziada et al. [13] used a one-dimensional numerical model to study the thermal behavior of a packed bed with the layered arrangement of different materials. The results show that the storage system can be arranged in layers using different materials to meet specific needs. Aly et al. [7] numerically studied the effect of the physical properties of the solid material on the thermal performance of the charging process. The results show that increasing the density or specific heat of the storage medium will increase the charging rate and storage capacity and reduce the rising rate of the bed temperature. Tuttle et al. [14] developed a new numerical simulation method to compare the storage performances of various materials. Due to the higher bulk mass and greater storage capacity, the metals' charging and discharging times are longer. Compared with the two, the thermal conductivity has less influence on the charging time. Ammar et al. [15] compared the performance of Tabla (a type of Egyptian clay) and rock through a computer program. The results showed that the heat stored in the Tabla bed is slightly higher than that of the rock bed, attributed to the higher specific heat and thermal conductivity. Mawire et al. [16] used a simplified one-dimensional single-phase model to study the thermal behavior of three different materials. Among them, fused silica glass has the best thermal stratification characteristics. Stainless steel has the highest energy stored, while aluminium oxide has the fastest charging rate. Eddemani et al. [17] used a transient two-phase heat transfer model to study the thermal behavior of three rocks (gabbro, quartzite and sandstone) in storage systems. The results show that gabbro has the best storage performance. In terms of physical experiments, Schlipf et al. [18] compared the thermal behaviors of quartz sand, basalt, and quartz gravel. The dynamic thermal behavior of quartz sand is slower due to the smaller particle size and larger bulk density. Audi [19] used a self-designed solar heating unit to test the storage performances of four different rocks. The results showed that tarsand and zeolite decomposed under the operational environment, while Jordanian basalt and limestone showed excellent stability and acceptable storage performance.

In summary, in the field of packed-bed sensible heat storage, the existing literature on the comparative study of different storage materials is often not comprehensive and systematic. They usually only focus on the characterization of thermophysical properties or the numerical simulation of thermal behavior but less on physical experiments. This paper comprehensively compared and analyzed the applicability of the three different materials as sensible heat storage materials. First, the three materials' chemical components and thermophysical properties were obtained by various characterization techniques to evaluate their potential as storage materials. Second, the cold tests of packed beds with three materials were conducted to study the air resistance characteristics. Finally, the energy storage tests of three materials beds under different operating conditions were carried out to explore the storage performances and thermocline evolution characteristics.

2. Experimental

2.1. Concepts of the storage system and experimental procedure

Fig. 1 illustrates the air-packed bed storage system and the charging-discharging cycle. The system is based on the direct contact between the heat transfer fluid (air) and storage materials inside the storage tank. A complete storage cycle contains a charging stage and a discharging stage. For charging, the hot air enters the storage tank from the top, releases heat to storage materials and finally flows out from the bottom. For discharging, the air flows in the opposite direction. Fig. 2 shows the experimental procedure.

2.2. Storage materials

In the previous work of our research group, sintered ore particles were proposed as a storage material. Meanwhile, aluminium oxide balls and rock gravel are widely favored by scholars as common storage materials. Therefore, the above three materials are selected as potential candidates for storage materials in the present work. Fig. 3 presents the three materials and their packed beds. The sinter comes from Zhejiang University-BHP Billiton Iron Ore Sintering Joint Research Center, with a 10–16 mm nominal diameter. The aluminium oxide balls were purchased from a ceramic manufacturer with a diameter of 13 mm. The rock gravel was purchased from a mineral product manufacturer with a 10–16 mm diameter. It can be seen from Fig. 3 that the diameter of crushed rock is slightly smaller than that of sintered ore particles.

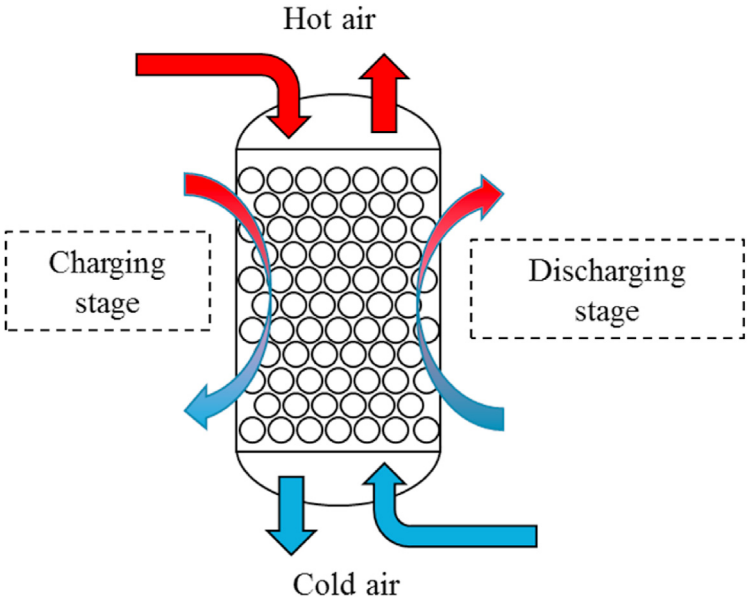

Fig. 1. Air-packed bed storage system and the charging-discharging cycle.

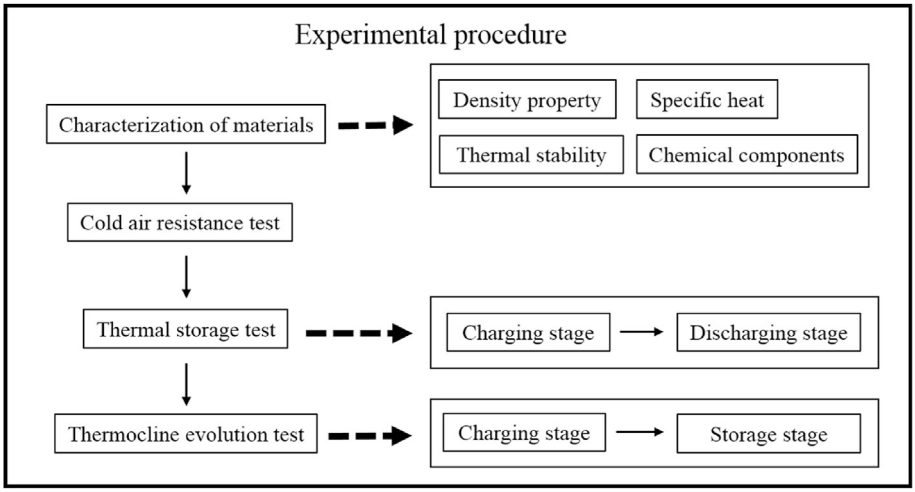

Fig. 2. Experimental procedure.

2.3. Characterization techniques

Apparent density is the ratio of the mass of a material to its apparent volume. The apparent volume is the solid volume plus the closed pore volume. Bulk density refers to the ratio of the mass of a material to the bulk volume. The bulk volume is the total volume, including voids between particles and pores inside particles. As defined above, the apparent density is usually greater than the bulk density. The apparent densities of the three materials were obtained by the Archimedes drainage method. The bulk density was measured by dividing the bulk mass and volume of the material in the storage tank. Bed voidage ε is calculated by the formula (1):

$$\varepsilon = 1 - \frac{\rho_b}{\rho_a} \tag{1}$$

A differential scanning calorimeter (DSC, TA Q200) was used to measure the material's specific heat at 0–400 °C. To evaluate the thermal stability of the materials, a synchronous thermal analyzer (TGA/DSC3+, Mettler, Switzerland) was used to perform the thermogravimetric test (TGA) on three samples in the range of 100–1000 °C (ten heating and cooling cycles). During the test, the heating and cooling rates were both 20 °C/min in an air atmosphere. Moreover, Shimadzu XRF-1800 was used to perform XRF tests on three samples to obtain the chemical compositions of materials. Before the test, the three materials (granular) were pulverized (about 75 μm) using a coal mill. Then put the powder samples in an oven at 105 °C for 24 h to remove the moisture.

2.4. Packed bed energy storage tests

Fig. 4 illustrates the schematic diagram of the packed-bed energy storage experimental system. The test used air as the heat transfer fluid. The experimental system was composed of a blower (fan power 0.55 kW), electric air heater (heating power 90 kW), storage tank, induced draft fan (fan power 90 kW), and piping system.

Table 1 shows the test conditions. The charging temperature

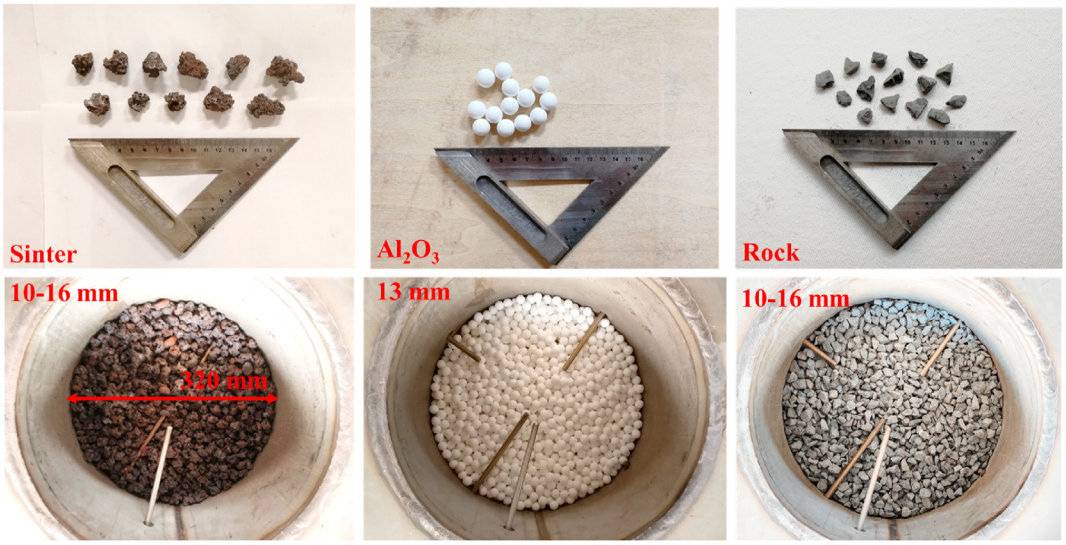

Fig. 3. Three kinds of energy storage materials and their packed beds in the storage tank.

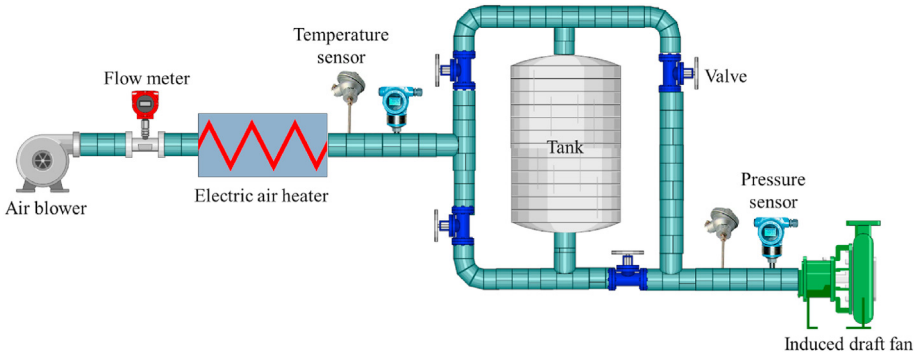

Fig. 4. Experimental system of packed bed thermal energy storage.

Table 1
Experimental conditions.

Case	V (m^3/h)	Material	Case	V (m^3/h)	Material	Case	V (m^3/h)	Material
A1	85	Sinter	B1	85	Al_2O_3	C1	85	Rock
A2	130		B2	130		C2	130	
A3	175 (1st)		B3	175 (1st)		C3	175 (1st)	
A4	175 (2nd)		B4	175 (2nd)		C4	175 (2nd)	
A5	175 (3rd)		B5	175 (3rd)		C5	175 (3rd)	

was 200 °C. Case A1-A5 used sinter as storage materials, B1—B5 used aluminium oxide, and C1—C5 used rock. It is worth pointing out that our research group has conducted lots of tests on the storage performances of sinter before, including case A1-A5. We found that the air flow and the cycle numbers have the most significant impact on the storage performances. Therefore, two other common storage materials were selected for tests to compare the differences and correlations of the storage performances of the three materials at different air flows and cycle numbers.

In the hot test, the induced draft fan was disconnected from the test system. For charging, the air supplied by the blower was heated to a predetermined temperature by the heater, then passed through the storage tank longitudinally from top to bottom, and finally was discharged to the atmosphere. To be consistent with the previous work, the charging stopped when the outlet air temperature of the tank reached 0.65 times of the predetermined charging temperature. Before discharging, the air heater needs to be cooled to a low-temperature state to ensure a low inlet air temperature and thus an excellent cooling effect on the bed. Furthermore, the air heater needs to be cooled to a low-temperature state to protect itself from being in high temperature for a long time. To maintain the consistency and coherence of the study, the air heater was cooled to 60 °C before discharging, which was consistent with the previous work. For discharging, the air heater was shut down. Low-temperature air was discharged into the atmosphere after passing through the tank from the bottom to the top. From the perspective of energy grade, air below 60 °C is of little use even for space heating. Therefore, the discharging stopped when the outflow temperature dropped below 60 °C. In the test, the air flow was changed by adjusting the valve opening of the blower. By setting

the heating program of the heater, the charging temperature can be controlled. Furthermore, cold tests were carried out on the three materials beds to study the air flow resistance characteristics. At this time, the blower was kept closed, and the induced draft fan provided airflow. The air flow is changed by adjusting the valve opening of the induced draft fan and the negative pressure of the pipeline using a control cabinet.

Fig. 5 shows the details of the tank and the thermocouple layout. The inner diameter of the tank is 320 mm, and the height is 850 mm. The height of the packed bed is 650 mm. The tank is manufactured with 310 S stainless steel, and its wall thickness is 10 mm. To reduce heat loss, the tank is equipped with a 250 mm castable insulation layer, and the piping system is equipped with a 150 mm insulation layer. The bed temperatures are measured using five thermocouples arranged at intervals of 100 mm inside the bed. The airflow temperatures at the inlet and outlet of the bed are measured with another two thermocouples. All temperatures are measured by K-type thermocouples with an accuracy of 1.5 °C. Agilent is used for data acquisition with a sampling interval of 10 s. The pressure sensors are used to measure the pressure difference between the inlet and outlet of the bed. The sampling interval is 1 s, and the sampling accuracy is 1 Pa. The static pressure and total pressure are measured by the Testo 435 micro-manometer with a sampling interval of 1 s and a sampling accuracy of 1 Pa. Based on Bernoulli's equation, the air velocity/flow rate can be obtained using the pressures data.

3. Results and discussion

3.1. Physical properties

Table 2 shows the density properties of the three materials. The apparent densities of sinter and aluminium oxide are significantly greater than that of rock. Meanwhile, the bulk density of sinter and rock are almost the same. As shown in Fig. 3, the aluminium oxide ball is close to the standard spherical shape, while the sinter and rock are irregular in shape. Due to the unique raw materials and

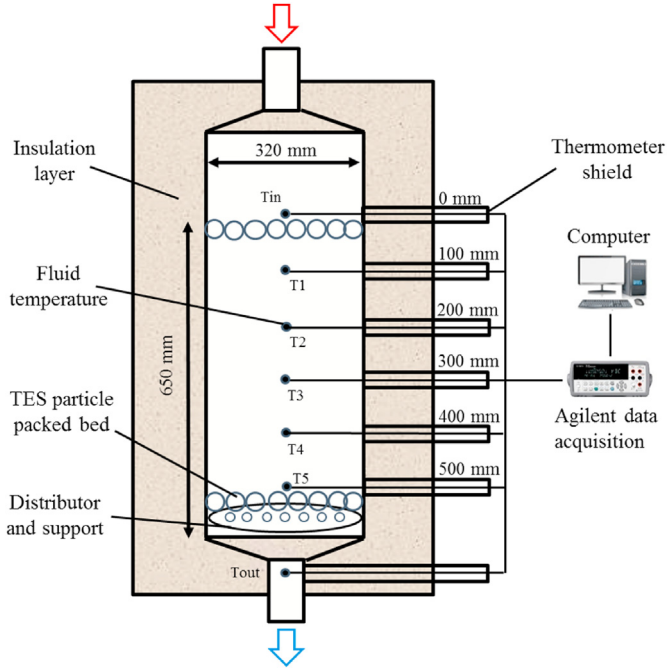

Fig. 5. Details of the storage tank and thermocouple layout inside the tank.

Table 2
Properties of various materials.

Materials	Sinter	Al_2O_3	Rock
Mass (kg)	83.84	117.03	82.06
Apparent density ρ_a (kg/m^3)	3727	3622	2762
Bulk density ρ_b (kg/m^3)	1605	2240	1581
Voidage of packed bed ε	0.569	0.382	0.428
Thermal conductivity (W/m·K)	2.5 [20,21]	30 [22]	2.5 [23]

production process, the surface of the sinter presents uneven, and the overall shape of the particles is random, while the rock appears to be close to flakes or pyramids. The particle size and shape affect the bed voidage. The voidage of the sinter bed is the largest, followed by rock bed, and the voidage of aluminium oxide bed is the smallest. The thermal conductivities of the three materials in the literature are also quoted in Table 2 for subsequent comparison and analysis. The thermal conductivity of sinter and rock is nearly the same, significantly lower than that of aluminium oxide.

For DSC measurement, most users choose a 5–20 °C/min heating or cooling rate [24]. Therefore, the DSC tests were conducted at 5 °C/min, 10 °C/min and 20 °C/min, respectively, in this current study. Fig. 6 plots the specific heat of three materials at different heating rates. The specific heat of each material increases as the temperature rises. The specific heat capacities of aluminium oxide and rock are similar and slightly higher than that of sinter. At 15–380 °C, the specific heat of aluminium oxide is about 0.74–1.18 J/(g·°C), similar to Cascetta's result [22]. The specific heat of rock is about 0.78–1.06 J/(g·°C), similar to Liu's result [25]. The specific heat of the sinter is about 0.71–0.92 J/(g·°C). Meanwhile, the influence of different heating rates on specific heat is minor. Specific heat capacity is the basic thermal physical property of materials, which does not change greatly with the heating rate. This theoretical analysis is consistent with our test results. For DSC measurement, sensitivity and resolution are a contradiction. The higher the heating rate, the higher the sensitivity and the lower the resolution. And vice versa. People generally choose a relatively slow heating rate to maintain good resolution while increasing the sample mass to improve sensitivity. In the present test, the specific heat results of the material increase slightly with increasing heating rate, which is attributed to a lower resolution resulting from more severe baseline drift. Therefore, we choose the measurement results at 5 °C/min as the final specific heat for the following discussion in this study. Based on 200 °C, the specific heat of sinter, aluminium oxide and rock are 0.8730 kJ/(kg·K), 0.9887 kJ/(kg·K), 0.9876 kJ/(kg·K), respectively. According to the apparent density in Table 2, the volumetric heat capacities of sinter, aluminium oxide and rock are 3253.7 kJ/(m^3·K), 3581.1 kJ/(m^3·K), and 2727.8 kJ/(m^3·K), respectively.

Fig. 7 delineates the thermogravimetric test results of three materials. The thermal stability of aluminium oxide is excellent at 100–1000 °C, and the mass change can be negligible (less than 0.5%). In the first cycle, the mass loss below 600 °C is attributed to the escape of moisture in the sample during heating. Although the sample was dried before the test, the fine powder on the sample's surface still adsorbed some moisture. Above 600 °C, the mass increases due to the oxidation of metallic components and the formation of new phases in the sample under the air atmosphere [26]. Starting from the cooling of the first cycle, the mass of aluminium oxide samples fluctuated slightly. This phenomenon may be attributed to two reasons. First, the rapid heating and cooling hinder the complete oxidation of the metallic parts [26]. Second, the buoyancy of the crucible itself in high temperature may cause measurement error, about 50 μg. The thermal stability of the sinter is good at 100–1000 °C, with a mass loss of about 5%. The mass loss

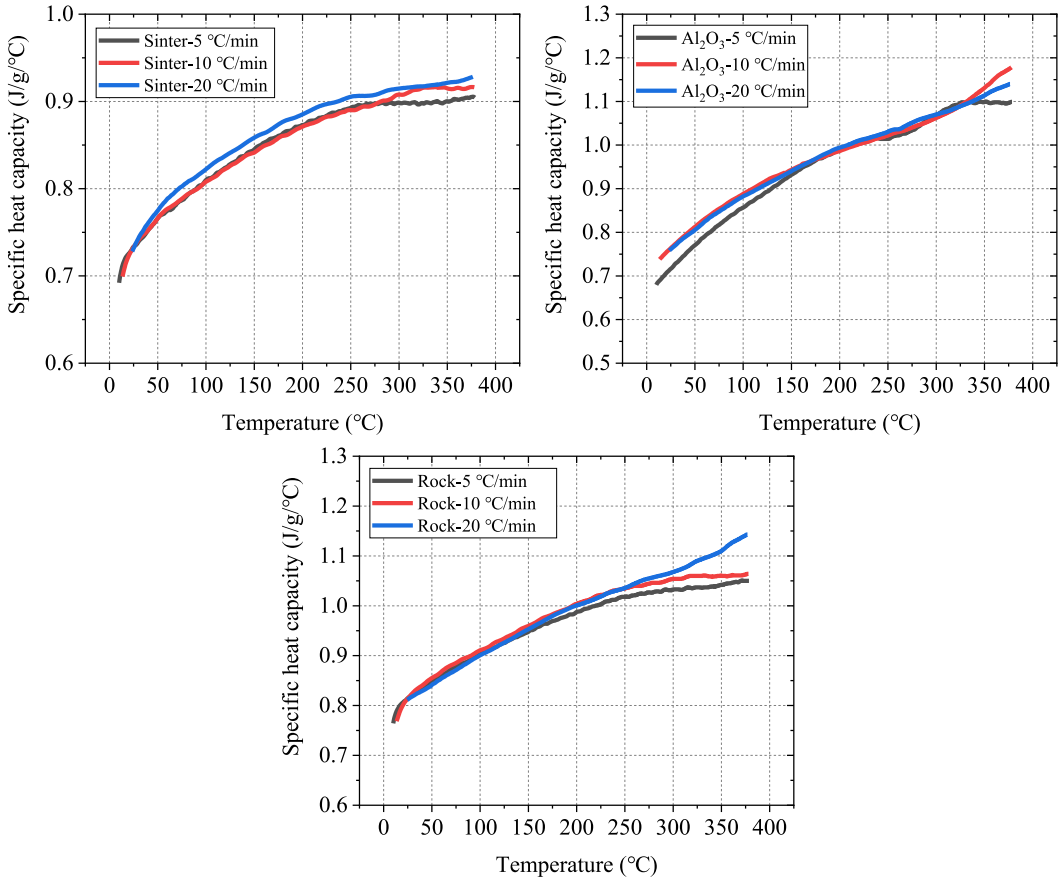

Fig. 6. Specific heat capacities of TES materials at different heating rates.

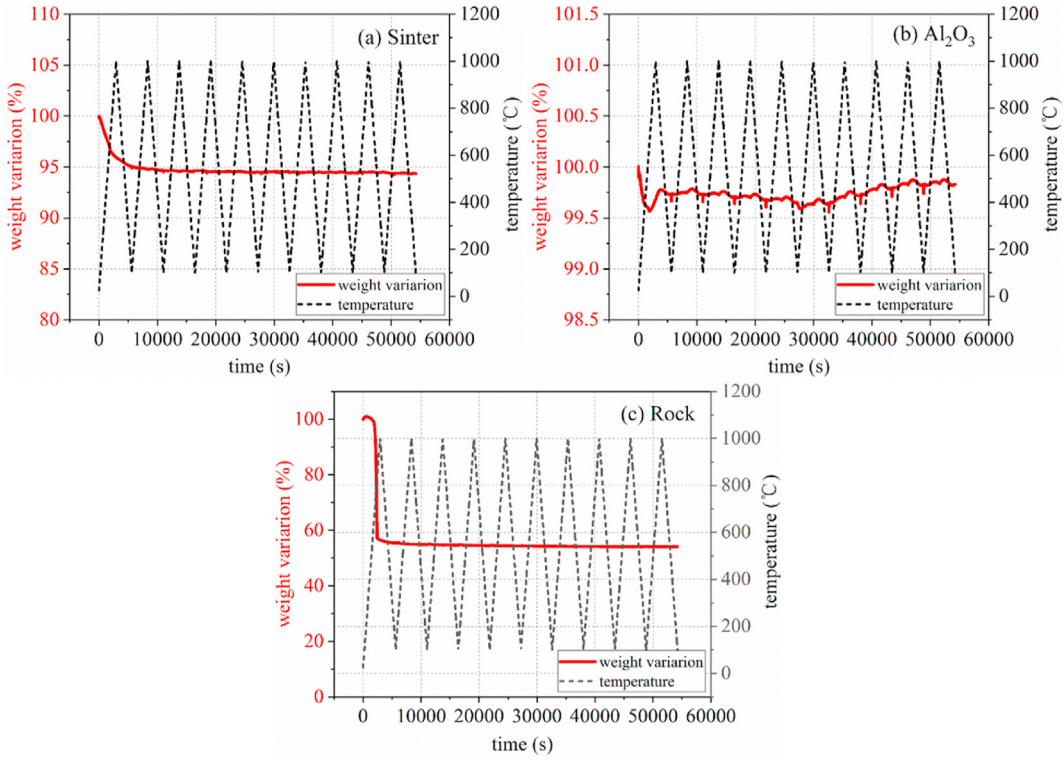

Fig. 7. TGA curves of various TES materials for ten thermal cycles (100–1000 °C).

is mainly attributed to the escape of moisture and gas volatilization [20] at high temperatures. It is worth pointing out that we only laid about 10 mg sinter samples in the crucible to ensure good heat transfer. This mass is relatively small with a relatively sizeable superficial area, which may result in a greater mass loss in thermogravimetric tests due to more surface moisture. In practical heat storage applications, the thermal stabilities of the materials should be better than the results of the current test. However, the rock's mass keeps unchanged below 580 °C, gradually decreases at 600 °C–800 °C, and finally stabilizes. In conclusion, the rock has poor thermal stability and can only store energy below 550 °C, while the aluminium oxide balls and sinter can store energy at an ultra-high temperature as high as 1000 °C.

Table 3 gives the chemical compositions of the three materials. As the primary raw material of blast furnaces, the four main components in sinter are calcium ferrite, iron oxide, ferroferric oxide, and silicate [27]. So its main element composition is Fe, O, Ca and Si. The purity of aluminium oxide is high, above 97%. For the rock, the percentages of Ca, O, and C are very high. Considering the weight loss of rock above 600 °C in thermogravimetric test, it is inferred that the main component of rock is calcium carbonate. The high-temperature decomposition reaction of calcium carbonate leads to rock decomposition in thermogravimetric tests.

3.2. Cold air resistance characteristics

Fig. 8 plots the pressure drop characteristics of the three beds at different air flows. Regardless of the material used, ΔP/H increases as the air superficial velocity increases, and the changing trend fits well with the binomial formula [28,29]. The fitting R^2 is greater than 0.99. Regardless of the material used, the reduced pressure drop ΔP/(HU) of the bed increases with the increase of the superficial air velocity, and the trend conforms to the linear change law [30,31]. The fitting R^2 is greater than 0.99. Under the same superficial air velocity, the pressure drop of the sinter bed is smaller than those of the aluminium oxide and rock bed. The pressure drops of the latter two beds are similar.

The result of Tian's test for 10–20 mm sintered ore particles has been added to Fig. 8(b) for comparison. The size of sinter particles is 10–16 mm in our work, so the pressure drop is larger than that of Tian's work. The trends of the ΔP/(HU) are consistent with the Tian' works, indicating that the current experimental results are accurate and reliable. On this basis, the permeability index JPU [32], which is widely used in iron ore sintering, and absolute permeability index k are used to characterize the air resistance characteristics of the beds.

$$JPU = \frac{V}{60A}\left(\frac{H}{\Delta \mathrm{p}}\right)^{0.6} \tag{2}$$

$$k = \frac{Uu\Delta \mathrm{y}}{\Delta p} \tag{3}$$

Fig. 9 shows the JPU and absolute permeability of the three beds at different air superficial velocities. The JPU and absolute permeability of the three beds first decrease rapidly and then gradually stabilize as the air superficial velocity increases. According to Ergon's equation, the voidage is the most significant factor affecting the bed permeability, followed by the average particle diameter. Besides, the particle shape also has a certain impact on permeability. From Table 2, the voidage of the sinter bed is significantly higher than those of the aluminium oxide bed and rock bed. Therefore, the JPU and absolute permeability of the sinter bed are higher than the latter two at the same air superficial velocity. Although the voidage of the aluminium oxide bed is slightly lower than that of the rock bed, the particle size of the rock seems to be smaller, and the shape is more irregular, which ultimately leads to the similar permeability of the two beds.

3.3. Energy storage performance

3.3.1. Evolution of bed temperature

Taking case C1 as a typical case, Fig. 10 shows the evolution of the bed temperature during charging and discharging. Clearly, the bed temperatures rise sequentially with time during charging. When the charging starts, a sharp thermocline is formed in the tank. There is a clear boundary between the top layer (high-temperature) and the bottom layer storage material (low-temperature). In the initial stage, due to the large temperature difference between the inlet air temperature and the bed temperature, the charging rate is faster, and the bed temperature rises rapidly. As the charging progresses, the bed temperature gradually rises, resulting in a gradual decrease of the temperature difference between the heat transfer fluid and the storage material. Hence, the charging slows down, and the bed temperature rises slowly. When the charging is over, the bed temperature at each axial position almost reaches the inlet air temperature. Similarly, the bed temperatures decrease sequentially with time during discharging. As the discharging progresses, the discharging rate gradually slows down.

3.3.2. Effect of air flow on storage performance

As shown in Fig. 10, the heat transfer fluid passes through the bed to transfer heat to the storage material. Meanwhile, the air temperature gradually decreases along the axial direction and finally drops to the outlet air temperature. Therefore, the outlet air

Table 3
Chemical components of various materials.

Material	Major components									
Sinter	Oxide	Fe_2O_3	CaO	SiO_2	Al_2O_3	MgO	TiO_2	MnO	P_2O_5	K_2O
	Wt (%)	83.44	8.86	4.01	1.85	1.07	0.35	0.28	0.08	0.06
	Element	Fe	O	Ca	Si	Al	Mg	Mn	Ti	K
	Wt (%)	77.31	9.92	7.85	2.30	1.19	0.77	0.28	0.27	0.06
Al_2O_3	Oxide	Al_2O_3	Fe_2O_3	CaO	SiO_2	Na_2O	Cr_2O_3	SO_3	Ga_2O_3	
	Wt (%)	97.37	1.64	0.34	0.29	0.25	0.04	0.04	0.02	
	Element	Al	O	Fe	Ca	Si	Na	Cr	Ga	S
	Wt (%)	71.84	24.84	2.26	0.46	0.26	0.23	0.05	0.03	0.03
Rock	Oxide	CO_2	CaO	MgO	SiO_2	Al_2O_3	Fe_2O_3	K_2O	SO_3	SrO
	Wt (%)	51.05	39.51	4.58	2.93	0.89	0.47	0.25	0.19	0.05
	Element	Ca	O	C	Mg	Si	Fe	Al	K	S
	Wt (%)	48.50	22.33	21.29	3.84	1.98	0.74	0.68	0.32	0.11

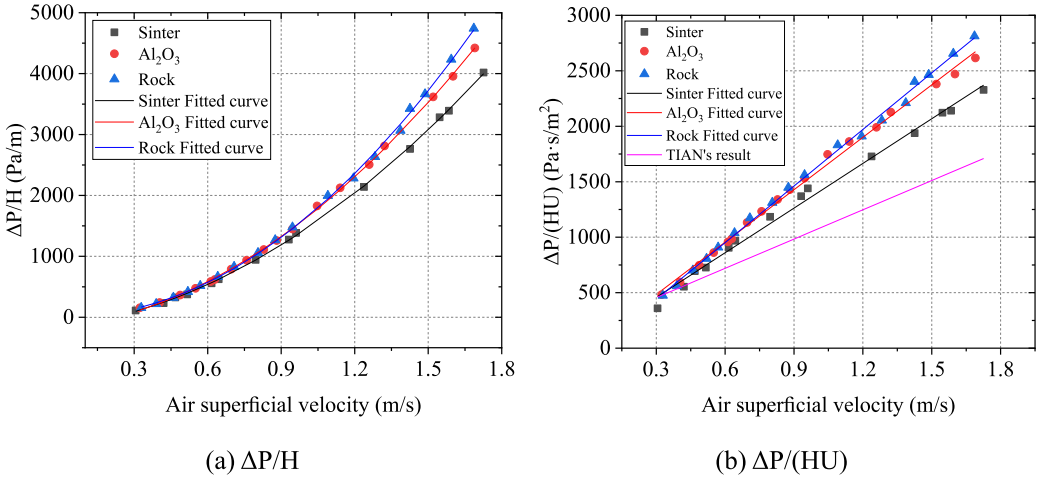

Fig. 8. Effect of U on ΔP/H and ΔP/(HU) for packed beds with different materials.

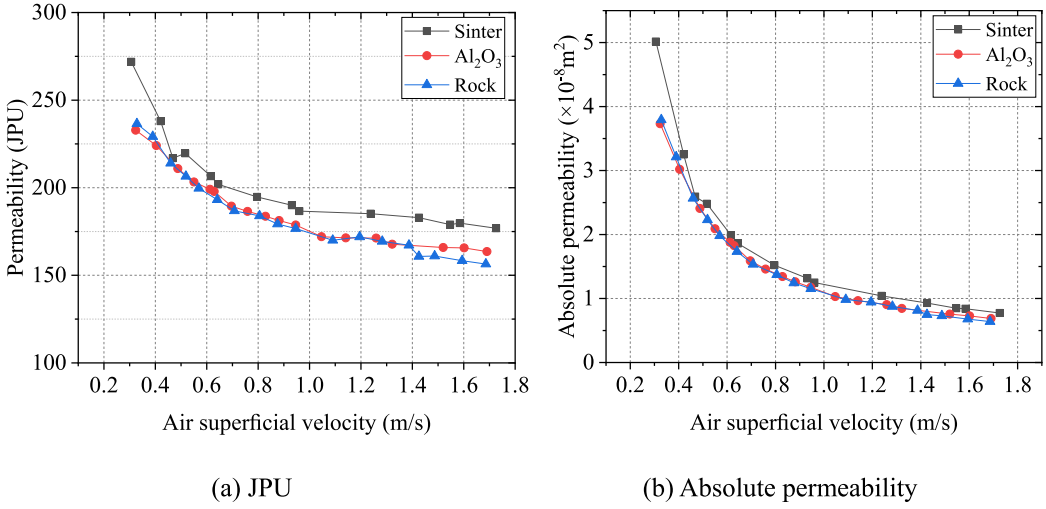

Fig. 9. Effect of U on JPU and absolute permeability for packed beds of three materials.

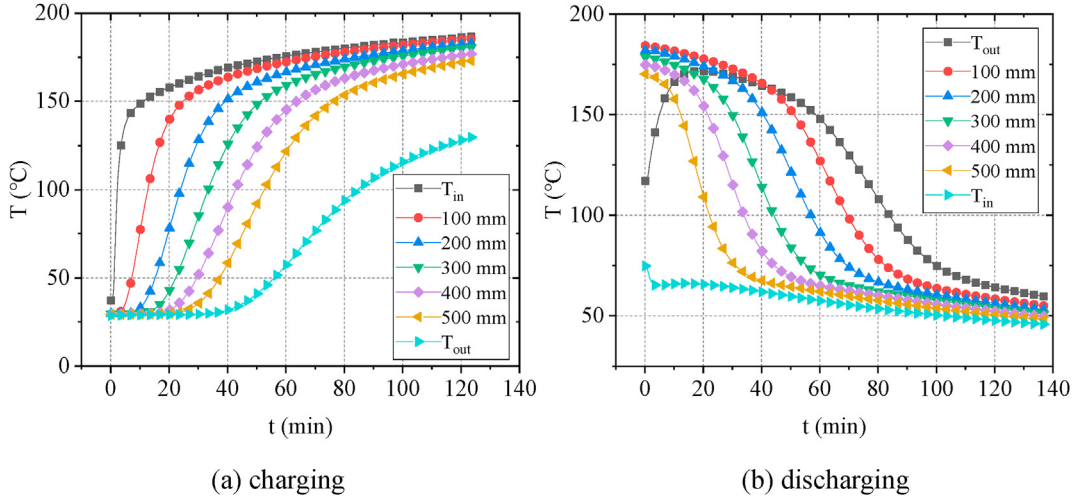

Fig. 10. Bed temperature evolution during charging and discharging.

temperature can represent the energy extraction capacity of the bed [33]. A higher outlet fluid temperature means a lower energy storage rate. Fig. 11 shows the evolutions of the inlet and outlet temperature of three beds under different air flows. As shown in Fig. 11 (a), the outlet temperature of the sinter bed rises earliest during charging, and the charging is completed first. The outlet temperature of the aluminium oxide bed rises at the latest, and the charging is completed at the latest. For the discharging, the aluminium oxide has the highest peak outlet temperature and the sinter has the lowest peak outlet temperature.

By comparing Fig. 11 (a), (b) and (c), it is found that the charging time and discharging time of the three materials decrease significantly with the increase of air flow. When the air flow increases from 85 m^3/h to 175 m^3/h, the charging time of sinter, aluminium oxide and rock decreases from 91.5 min, 191.2 min and 124.3 min−39.5 min, 80.8 min and 49.3 min, respectively, and the discharging time decreases from 98 min, 198.2 min and 136.8 min−42 min, 89.2 min and 55.5 min respectively. This decline is because the greater the air flow, the greater the air superficial velocity in the tank. The larger air superficial velocity enhances the heat exchange between the heat transfer fluid and the storage medium [1]. Moreover, the decreases of charging time of different

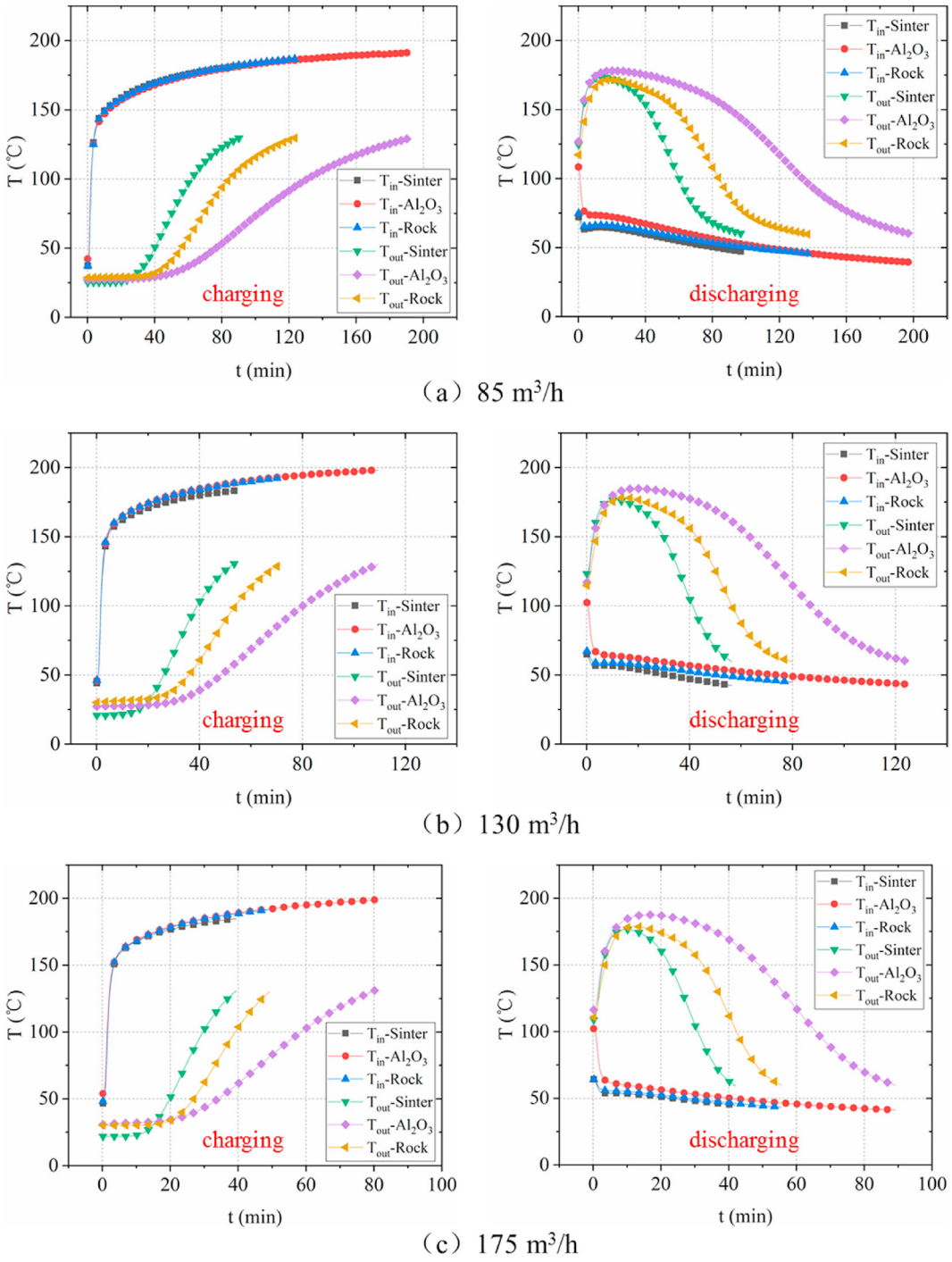

Fig. 11. Evolutions of inlet and outlet temperature of various materials beds at different air flows.

materials with the increase of air flow are nearly the same. When the air flow increases from 85 m^3/h to 130 m^3/h, the charging times decrease to 57%–59% of the original values. When the air flow increases from 85 m^3/h to 175 m^3/h, the charging times decrease to 39.6%–43% of the original values. The decrease extent of charging time declines gradually, and further increasing the air flow will have less influence on the charging time.

Fig. 12 shows the evolutions of energy stored and energy released of the three materials over time. The air flow is 85 m^3/h. The charging curves of the three materials almost coincide in the initial stage of charging, indicating that all the three materials can cool the heat transfer fluid to the ambient temperature, and the charging rates are the same. With the progress of charging, the charging rate of the sinter starts to lag behind the other two materials at about 40 min. At about 60 min, the charging rate of the rock begins to lag behind that of the aluminium oxide. The final energy stored of sinter, rock and aluminium oxide are 4.71 kWh, 6.81 kWh and 10.80 kWh, respectively. The heat stored is affected by the density and specific heat of the solid medium [7,14,18]. It can be seen from Table 2 that the bulk mass of sinter and rock is similar, while Fig. 6 shows that rock has a higher specific heat than sinter, so the energy stored of rock is larger than that of sinter. As the specific heat and bulk mass of aluminium oxide are higher than those of sinter and rock, the energy stored of aluminium oxide is significantly greater than that of the other two [7,14,18]. Furthermore, it can be seen that the charging time is mainly affected by the heat capacity of the bed, and the high thermal conductivity of aluminium oxide does not seem to reduce the charging time significantly. The changing trend of discharging curve is consistent with that of the charging curve. Since the inlet air temperature is about 60 °C during discharging, the temperature difference between the storage material and the heat transfer fluid is smaller than the charging, so the discharging power is smaller. Due to heat loss and incomplete heat release, the final heat released is less than the heat stored.

In order to quantitatively evaluate the storage performances of three materials, charging efficiency, discharging efficiency and cycle efficiency are introduced [34,35]. Charging efficiency is the ratio of the total heat stored in the tank to the sum of the input energy and the pumping work consumed by the airflow through the bed during charging. Discharging efficiency is the ratio of the heat released from the tank to the sum of heat stored and the pumping work during discharging. Cycle efficiency, namely energy recovery efficiency, is a key indicator for evaluating energy storage performance of storage materials and storage systems. It is defined as the ratio of the heat released during discharging to the total energy consumption in a complete storage cycle. The total energy consumption contains the input energy and the pumping work during charging and discharging.

$$\eta_{charging} = \frac{\int_{t_o}^{t_{end}} Q_{stored} \cdot dt}{E_{input} + E_{pump}} \tag{4}$$

$$\eta_{discharging} = \frac{\int_{t_o}^{t_{end}} Q_{release} \cdot dt}{Q_{stored} + E_{pump}} \tag{5}$$

$$\eta_{cycle} = \frac{\int_{t_o}^{t_{end}} Q_{release} \cdot dt}{E_{input} + E_{pump(charging)} + E_{pump(discharging)}} \tag{6}$$

Where, Q_{stored} is the heat stored in the tank during charging, E_{input} is the input energy, E_{pump} is the pumping work consumed by the airflow through the bed, $Q_{release}$ is the heat released during discharging, and they are defined below.

$$Q_{stored} = mc_{pair} \cdot \Delta t \cdot (T_{in} - T_{out}) \tag{7}$$

$$E_{input} = \int_{t_o}^{t_{end}} \int_{T_o}^{T_{end}} m \cdot c_{pair} dT \cdot dt \tag{8}$$

$$E_{pump} = \int_{t_o}^{t_{end}} \frac{m}{\rho_{air}} \Delta p dt \tag{9}$$

$$Q_{release} = mc_{pair} \cdot \Delta t \cdot (T_{out} - T_{in}) \tag{10}$$

Where, m is air mass flow, c_{pair} is specific heat capacity of air, t is

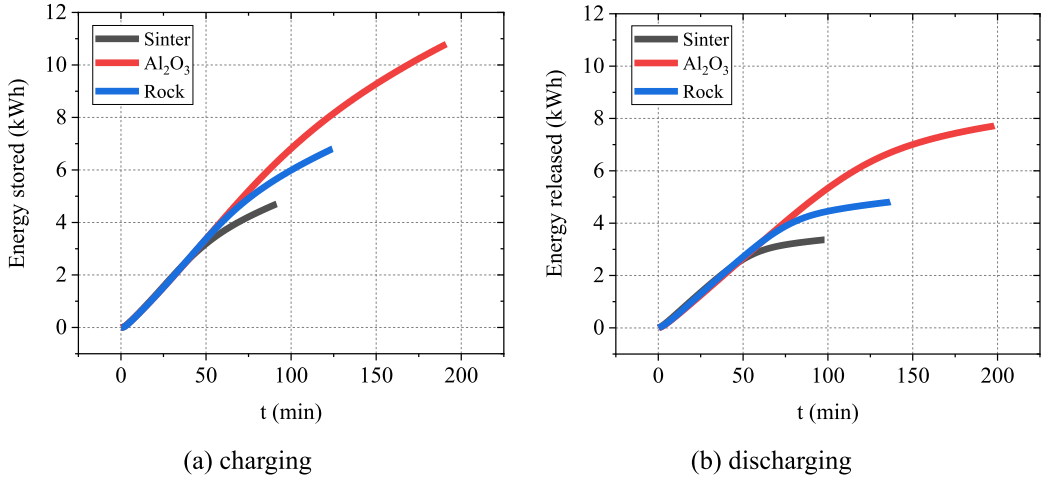

Fig. 12. Evolutions of energy stored and energy released of various materials beds.

time, T_{in} and T_{out} are air temperature at the inlet and outlet of the tank, respectively.

Fig. 13 shows the charging efficiency, discharging efficiency and cycle efficiency of various materials at different air flows. The charging efficiencies of the sinter and rock increase as the air flow increases because the larger air flow leads to a higher heat transfer rate and a shorter charging time, so the heat loss is greatly reduced. Besides, the improvement degree of the charging efficiency decreases gradually with the increase of the air flow, indicating that it is impossible to improve the charging efficiency endlessly by increasing the air flow. On the one hand, increasing the air flow enhances the turbulence and pressure drop in the bed, which will increase the pumping work consumption. On the other hand, increasing the air superficial velocity reduces the time for airflow to pass through the bed. This change means that the heat transfer time between the heat transfer fluid and the storage medium is reduced, which is not conducive to improving the heat transfer effect. This inference can be proved by the fact that the charging efficiency of aluminium oxide bed decreases with the further increase of air flow in Fig. 13. The discharging efficiency of the three materials increases with the increase of the air flow, and the increase amplitude decreases gradually. When the air flow is increased, the discharging time is reduced and the heat loss is reduced. The cycle efficiency of the three materials increases with the increase of air flow. There is little difference in the overall cycle efficiency of the three materials at low and medium air flow. At the high flow rate, the cycle efficiency of the rock is the highest, followed by aluminium oxide, and the cycle efficiency of sinter is the lowest.

3.3.3. *Effect of cycle number on storage performance*

Fig. 14 shows the evolutions of the inlet and outlet temperature of three materials under different cycle times. Compared with the first cycle, the initial values of the bed temperatures in the last two cycles are higher, and thus the charging time is shorter. This result is because of the incomplete heat release in the current test. That is, after the discharging is finished, there is still residual heat remaining in the bed. From the first cycle to the third cycle, the charging time of sinter, aluminium oxide and rock decreased from 39.5 min, 80.8 min and 49.3 min−34 min, 67.7 min and 43.3 min, respectively. It is also noted that the cycle number has little effect on the discharging curve, indicating that the cycle number does not affect the discharging performance. Moreover, the temperature curves of the second and the third cycles almost coincide, indicating that the system gradually enters a stable operation state from the second cycle.

Fig. 15 shows the charging efficiency, discharging efficiency and cycle efficiency of three materials under different cycle times. No matter what kind of storage material is used, the initial bed temperature in the subsequent cycle is higher than that in the first cycle due to incomplete heat release, so the charging efficiency in the subsequent cycle is lower. For the discharging, due to the incomplete heat release, the discharging efficiency of the first cycle is much lower than those of the subsequent cycles. The heat

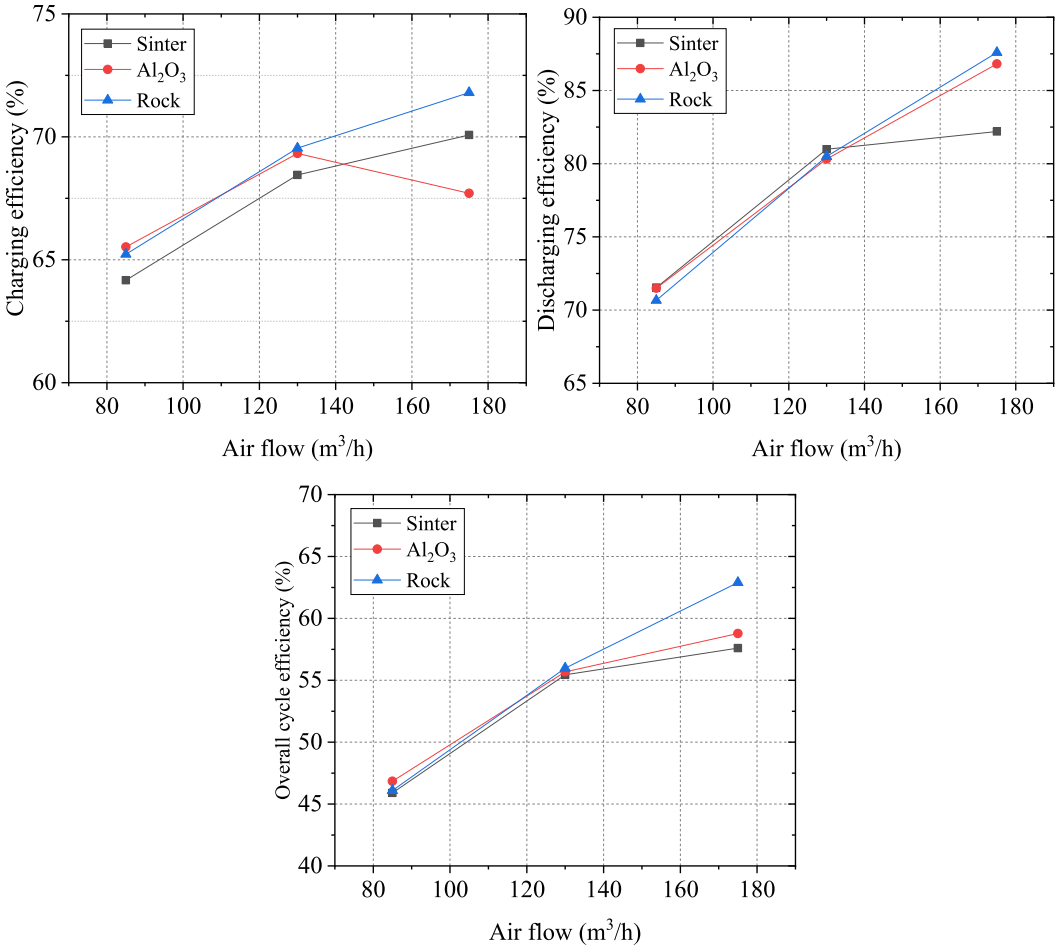

Fig. 13. Efficiency of various materials beds at different air flows.

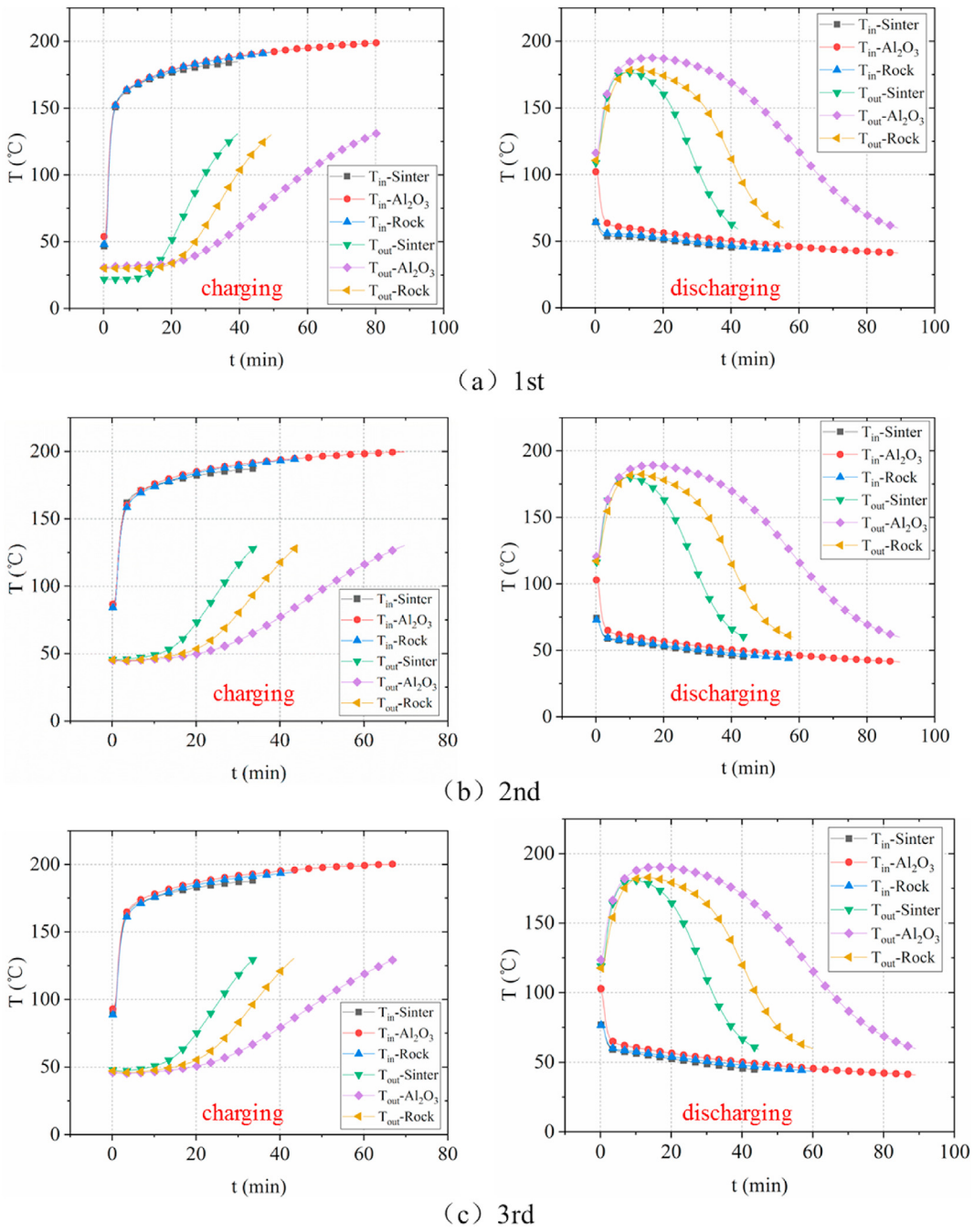

Fig. 14. Evolutions of inlet and outlet temperature of three materials beds at different cycle numbers.

accumulated in the system in the previous cycle is gradually released in the subsequent cycle, so the discharging efficiency of the subsequent cycle is slightly higher than 100%. In general, the overall cycle efficiency of all materials increases with the increase of cycle times, and the increase amplitude decreases gradually. The system gradually enters a stable operation state from the third cycle. For the third cycle, the overall cycle efficiency of sinter, aluminium oxide and rock is 66.8%, 69.3% and 73.7%, respectively.

3.3.4. Thermocline evolution characteristics

Stratification number (Str) is used to quantitatively evaluate the thermal stratification performance of packed beds [36–38]. The Str is the ratio of the average temperature gradient at any time t to the maximum average temperature gradient during charging.

$$Str = \frac{\overline{\left(\frac{\partial T}{\partial y}\right)_t}}{\left(\frac{\partial T}{\partial y}\right)_{max}} \tag{11}$$

$$\overline{\left(\frac{\partial T}{\partial y}\right)_t} = \frac{1}{I-1} \cdot \left[\sum_{i=1}^{I-1}\left(\frac{T_{i+1}-T_i}{\Delta y}\right)\right] \tag{12}$$

$$\overline{\left(\frac{\partial T}{\partial y}\right)_{max}} = \frac{T_{in}-T_{ini}}{(I-1)\cdot\Delta y} \tag{13}$$

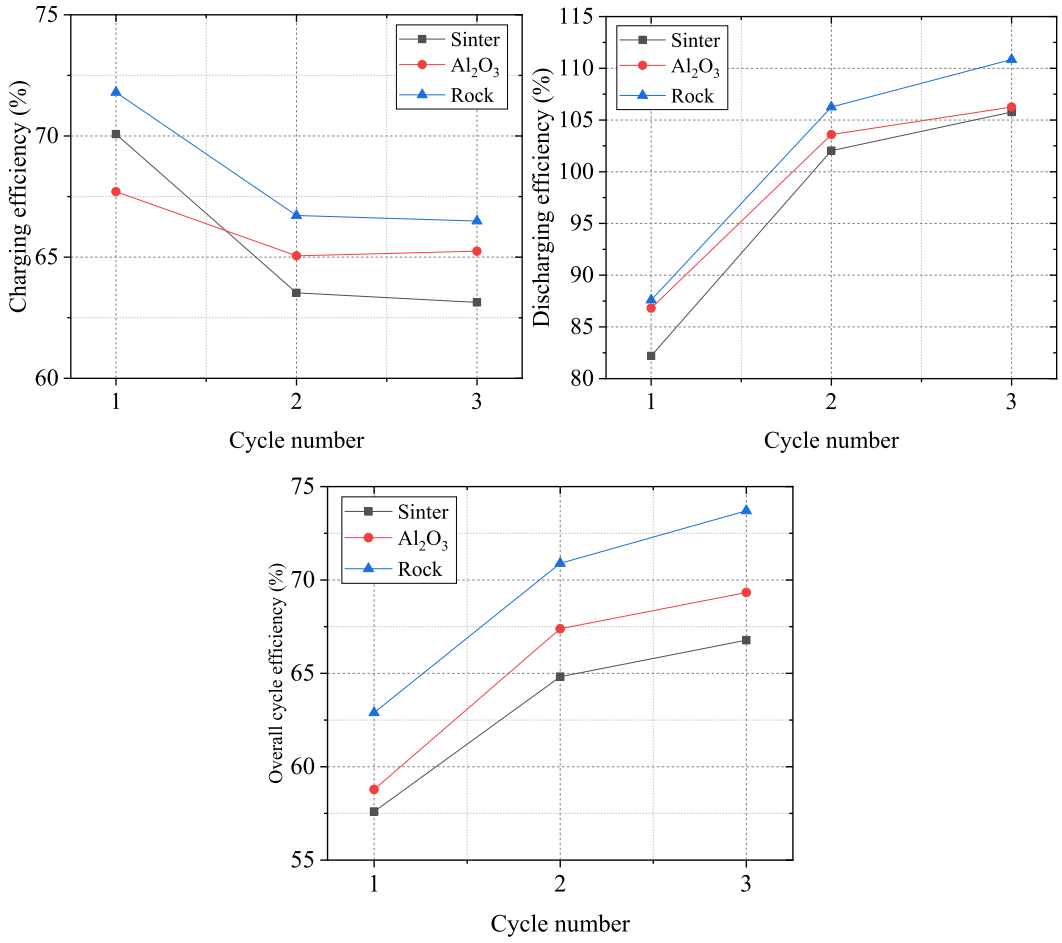

Fig. 15. Efficiency of various materials beds at different cycle numbers.

Fig. 16 shows the evolution of the Str of the three materials during charging. Three different air flow cases are located on the left, and three different cycle number cases are located on the right. As shown in the figure, the Str in each case increases rapidly at first and then gradually decreases with time. The changing trend of Str represents the formation and decay of thermocline in the bed. In the initial stage of charging, the high-temperature fluid first transfers heat to the storage material at the inlet, and the thermocline is formed and rapidly becomes sharp. As the charging proceeds, the temperature difference between the high-temperature fluid and the storage material at the inlet decreases, and the heat transferred decreases. After flowing through the top layer of particles, the air has residual thermal energy to heat the bottom particles that are still in a low temperature state. As a result, the heat transfer front (rapid heat transfer area, i.e., the area with the largest local temperature difference between heat transfer fluid and storage medium) gradually transfers downward, and the thermocline gradually disappears. Besides, the peak Str of rock and aluminium oxide is similar, higher than that of sinter, and the peak arrival time is later than that of sinter. The thermal stratification characteristics of the bed are affected by the physical properties of the material and bed voidage. The sinter bed has the lowest heat capacity and highest voidage, so the Str peak is the lowest and arrives at the earliest. Aluminium oxide bed has the highest heat capacity and lowest voidage, so the peak Str arrives at the latest. The rock bed has a low voidage and the smallest particle size, so the peak Str is the highest.

By comparing Fig. 16 (a), (b) and (c), the thermal stratification characteristic deteriorates when the air flow increases [37,38]. Specifically, the peak Str decreases and the time of reaching the peak Str is advanced. This change is because when the air flow increases, the residence time of the heat transfer fluid in the bed becomes less, although the convective heat transfer coefficient increases. Therefore, after passing through the top layer of particles, the fluid still has residual thermal energy to heat the lower layer of particles. In general, the heat transfer fluid tends to heat the bed uniformly in the axial direction at high air flow, while the heat transfer fluid tends to heat the top particles preferentially at low air flow. By comparing Fig. 16 (d), (e) and (f), the peak Str in the last two cycles are nearly the same, which is significantly smaller than that in the first cycle. In the last two cycles, the corresponding time of peak Str is nearly the same, slightly earlier than the first cycle. Incomplete heat release increases the initial bed temperature in the subsequent cycle, so the temperature difference between the heat transfer fluid and storage material is smaller, and the thermal stratification characteristics worsen.

The storage system has a certain period of heat storage stage between charging and discharging in industrial applications. In the heat storage stage, the bed temperature will reach a new thermal equilibrium state, and the thermocline will evolve and degrade gradually, resulting in irreversible exergy loss. It is very significant to study the thermocline evolution characteristics in heat storage stage for guiding the field application of energy storage industry. This section focuses on the thermocline evolution in the three beds.

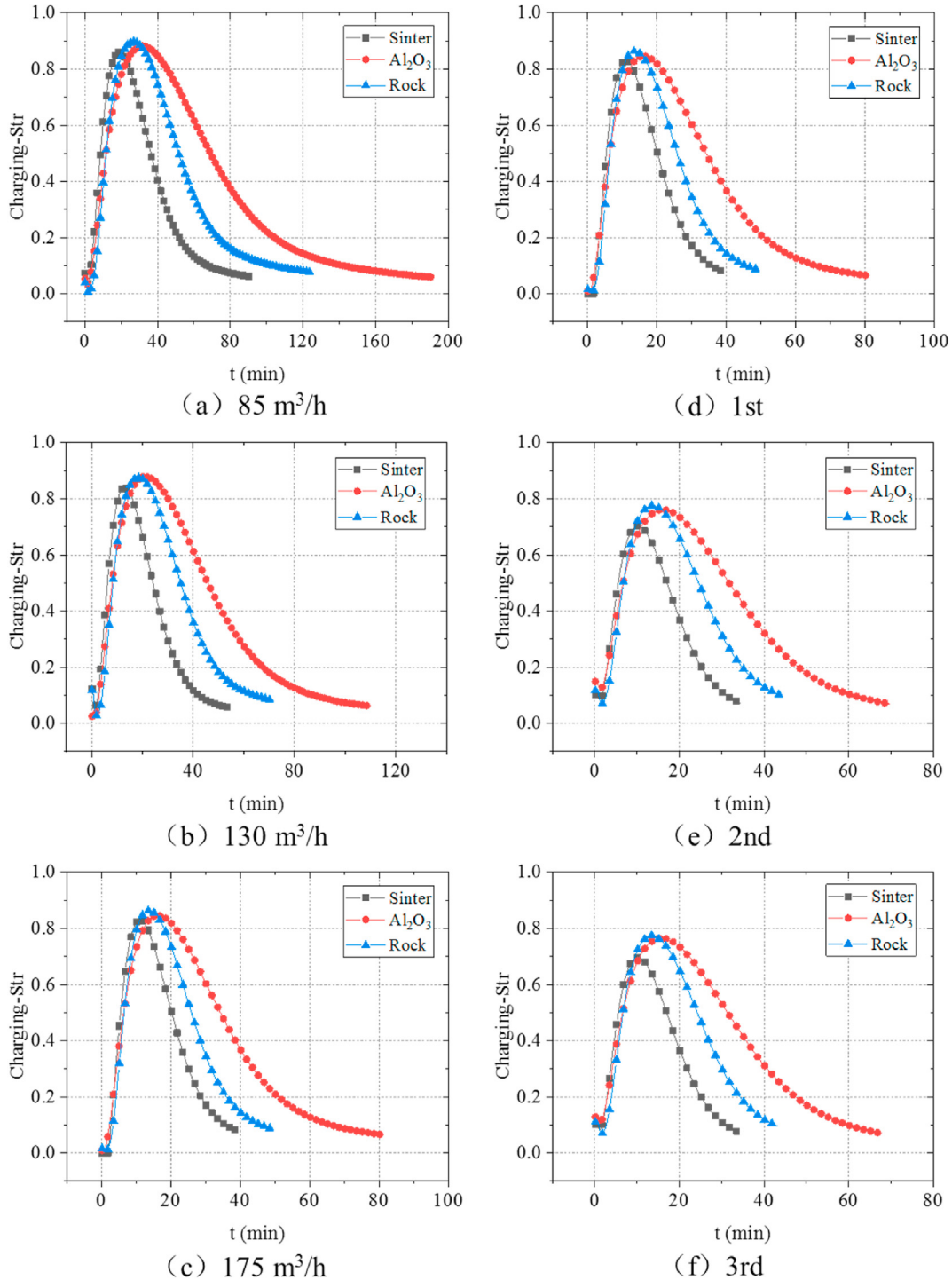

Fig. 16. Evolution of Str of various materials beds during charging.

The charging temperature is 300 °C, and the air flow is 85 m^3/h. In this test, charging is stopped at 20 min, 33.83 min and 26 min for sinter, aluminium oxide and rock bed, respectively. According to preliminary experimental results, the Str can reach the peak value at the corresponding moment mentioned above.

Fig. 17 shows the thermocline evolution characteristics of various materials after stopping charging. The Str decays the slowest in aluminium oxide bed, followed by rock bed and the fastest in sinter bed. The aluminium oxide and rock beds have smaller voidage, which dramatically weakens the flow of air within the beds, and heat transfer slows down, so the thermocline deceases more slowly. Moreover, the aluminium oxide bed and rock bed have higher heat capacities, especially the aluminium oxide, which makes the energy density higher, and thus the temperature change is smaller for the same heat transferred and the Str changes more slowly. It is noteworthy that the aluminium oxide has a significantly higher thermal conductivity, but this does not cause the Str to decay faster in the aluminium oxide bed. This

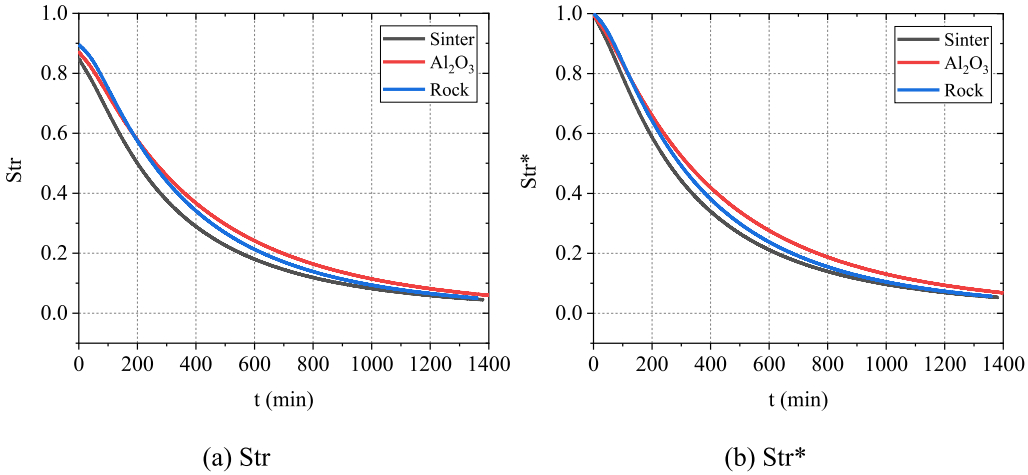

Fig. 17. Thermocline evolution characteristics of various materials beds.

phenomenon indicates that the thermal conductivity of the material has little effect on the thermocline evolution. As the initial Str of different material beds are different, it is not favorable for comparison. Fig. 17(b) shows the evolution characteristics of Str*, which is Str after the normalization based on the initial value. As shown in Fig. 17(b), the Str* can better characterize the thermocline evolution characteristics in different materials beds. The thermal stratification of aluminium oxide bed attenuated the slowest, followed by rock bed, and sinter bed attenuated the fastest. It takes 559.0 min, 499.5 min and 450.5 min for the Str* to decrease to 30% of the original value in aluminium oxide, rock and sinter bed, respectively. In conclusion, aluminium oxide bed have the best thermocline retention characteristics, followed by rock and sinter bed under current experimental conditions.

4. Conclusions

In this paper, the physical properties of sinter, aluminium oxide ball and rock were characterized and the packed bed heat storage tests were carried out to study their applicability as energy storage materials. The main conclusions are as follows:

(1) The volume heat capacity of sinter at 200 °C is 3253.7 kJ/(m^3·K), which is between aluminium oxide and rock. The sinter and aluminium oxide can withstand the high temperature of 1000 °C, while the rock in the present experiment has poor thermal stability above 600 °C. Considering the high cost of aluminium oxide, rock is the best choice for heat storage below 550 °C, while sinter is the best alternative material in the ultra-high temperature above 600 °C.
(2) The heat storage experiments of packed beds show that the bed heat capacity and the voidage, which are related to the bulk density and the specific heat of the material, are the key factors affecting the thermal behavior of the bed, while the thermal conductivity of the material has little effect. Increasing the air flow can significantly increase the average charging power, reduce the charging time, and improve the overall cycle efficiency. At low and medium air flow, the cycle efficiency of the three materials has little difference. Under the high air flow of 175 m^3/h, the cycle efficiency of rock, aluminium oxide and sinter bed is 73.7%, 69.3% and 66.8%, respectively.
(3) The thermocline characteristics of the packed bed are affected by the thermophysical properties of the material and the bed structure. Larger bed heat capacity and smaller voidage are favorable for the formation and maintenance of sharper thermocline.

Author contributions

Hao Zhou: Project administration, Supervision, Funding acquisition, Conceptualization, Resources. **Zhenya Lai**: Review, Methodology, Investigation, Data Curation, Validation, Formal analysis, Software, Visualization, Writing - original draft, Writing - Review & Editing. **Kefa Cen**: Project administration, Supervision.

Declaration of competing interest

The authors declare that they have no known competing financial interests or personal relationships that could have appeared to influence the work reported in this paper.

Acknowledgements

This work was supported by the National Natural Science Foundation of China (52036008).

References

[1] Agrawal Piyush, Gautam Abhishek, Kunwar Anshul, Kumar Manoj, Chamoli Sunil. Performance assessment of heat transfer and friction characteristics of a packed bed heat storage system embedded with internal grooved cylinders [J]. Sol Energy 2018;161:148–58.
[2] Chai Lei, Wang Liang, Jia Liu, Yang Liang, Chen Haisheng, Tan Chunqing. Performance study of a packed bed in a closed loop thermal energy storage system [J]. Energy 2014;77:871–9.
[3] Fernandes D, Pitié F, Cáceres G, Baeyens J. Thermal energy storage: "How previous findings determine current research priorities". J Energy 2012;39:246–57.
[4] Mawire A, Mc Pherson M, van den Heetkamp RRJ, Taole SH. Experimental volumetric heat transfer characteristics between oil and glass pebbles in a small glass tube storage [J]. Energy 2010;35:1256–62.
[5] Kuravi Sarada, Trahan Jamie, Yogi Goswami D, Rahman Muhammad M, Stefanakos Elias K. Thermal energy storage technologies and systems for concentrating solar power plants [J]. Prog Energy Combust Sci 2013;39:285–319.
[6] Kocak Burcu, Paksoy Halime. Performance of laboratory scale packed-bed thermal energy storage using new demolition waste based sensible heat materials for industrial solar applications [J]. Sol Energy 2020;211:1335–46.
[7] Aly SL, El-Sharkawy AI. Effect of storage medium on thermal properties of packed beds [J]. Heat Recovery Syst CHP 1990;10:509–17.
[8] Gautam Abhishek, Saini RP. A review on technical, applications and economic

aspect of packed bed solar thermal energy storage system [J]. J Energy Storage 2020;27:101046.
[9] Brosseau Doug, Kelton John W, Ray Daniel, Edgar Mike, Chisman Kye, Emms Blaine. Testing of thermocline filler materials and molten-salt heat transfer fluids for thermal energy storage systems in parabolic trough power plants [J]. J Sol Energy Eng 2005;127:109–16.
[10] Allen KG, von Backström TW, Kröger DG, Kisters AFM. Rock bed storage for solar thermal power plants: rock characteristics, suitability, and availability [J]. Sol Energy Mater Sol Cells 2014;126:170–83.
[11] Hrifech Soukaina, Hassan Agalit, Jarni Abdelmajid, Mouguina El Mostafa, Grosu Yaroslav, Faik Abdessamad, , El Ghali Bennouna, Mimet Abdelaziz. Characterization of natural rocks as filler materials for medium-temperature packed bed thermal energy storage system [J]. J Energy Storage 2020;32:101822.
[12] Calderon-Vasquez Ignacio, Segovia Valentina, Cardemil Jose M, Rodrigo Barraza. Assessing the use of copper slags as thermal energy storage material for packed-bed systems [J]. Energy 2021;227:120370.
[13] Ziada MA, Abdel Rehim ZS. Thermal analysis of energy storage in packed beds of multilayer storing medium [J]. Energy Sources 1998;20(3):209–22.
[14] Tuttle Jacob F, White Nate, Mohammadi Kasra, Powell Kody. A novel dynamic simulation methodology for high temperature packed-bed thermal energy storage with experimental validation [J]. Sustain Energy Technol Assessments 2020;42:100888.
[15] Ammar ASA, Ghoneim AA. Optimization of a sensible heat storage unit packed with spheres of a local material [J]. Renew Energy 1991;1(1):91–5.
[16] Mawire A, Mc Pherson M, van den Heetkamp RRJ, Mlatho SJP. Simulated performance of storage materials for pebble bed thermal energy storage (TES) systems [J]. Appl Energy 2009;86:1246–52.
[17] Eddemani Aicha, Bammou Lahcen, Tiskatine Rachid, Ahmed Aharoune, Bouirden Lahcen, Ahmed Ihlal. Evaluation of the thermal performance of the air-rock bed solar energy storage system [J]. Int J Ambient Energy 2019:1–29.
[18] Schlipf D, Schicktanz P, Maier H, Schneider G. Using sand and other small grained materials as heat storage medium in a packed bed HTTESS [C]. International Conference on Concentrating Solar Power and Chemical Energy Systems, Solar PACES 2014. Energy Procedia 2015;69:1029–38.
[19] Audi Mahmoud S. Experimental study of a solar space heating model using Jordanian rocks for storage [J]. Energy Convers Manag 1992;33(9):833–42.
[20] Tian Fuyou, Huang Lianfeng, Fan Liwu, Weng Yuankai, Ying Xiaoyuan, Yu Zitao, Cen Kefa. A comprehensive characterization on the structural and thermophysical properties of sintered ore particles toward waste heat recovery applications [J]. Appl Therm Eng 2015;90:1007–14.
[21] Feng Junsheng, Dong Hui, Gao Jianye, Li Hanzhu, Liu Jingyu. Numerical investigation of gas-solid heat transfer process in vertical tank for sinter waste heat recovery [J]. Appl Therm Eng 2016;107:135–43.
[22] Cascetta Mario, Cau Giorgio, Puddu Pierpaolo, Serra Fabio. A study of a packed-bed thermal energy storage device: test rig, experimental and numerical results [J]. 69th Conference of the Italian Thermal Engineering Association, ATI 2014. Energy Proc 2015;81:987–94.
[23] Meier Anton, Winkler Christian, Wuillemin Daniel. Experiment for modeling high temperature rock bed storage. J] Solar Energy Materials 1991;24:255–64.
[24] Richardson MJ. Quantitative aspects of differential scanning calorimetry [J]. Thermochim Acta 1997;300:15–28.
[25] Jia Liu, Wang Liang, Yang Liang, Yue Lei, Chai Lei, Sheng Yong, Chen Haisheng, Tan Chunqing. Experimental study on heat storage and transfer characteristics of supercritical air in a rock bed [J]. Int J Heat Mass Tran 2014;77:883–90.
[26] Agalit H, Zaria N, Maaroufi M. Thermophysical and chemical characterization of induction furnace slags for high temperature thermal energy storage in solar tower plants [J]. Sol Energy Mater Sol Cell 2017;172:168–76.
[27] Zhou H, Ma PN, Lai ZY, Zuo YH, Xing YJ, Shi H, Cen KF. Harmless treatment of waste selective catalytic reduction catalysts during iron ore sintering process [J]. J Clean Prod 2020;275:122954.
[28] Feng Junsheng, Dong Hui, Dong Hongda. Modification of Ergun's correlation in vertical tank for sinter waste heat recovery [J]. Powder Technol 2015;280:89–93.
[29] Feng Junsheng, Dong Hui, Liu Jingyu, Liang Kai, Gao Jianye. Experimental study of gas flow characteristics in vertical tank for sinter waste heat recovery [J]. Appl Therm Eng 2015;91:73–9.
[30] Tian Fuyou, Huang Lianfeng, Fan Liwu, Qian Hongliang, Gu Jiaxi, Yu Zitao, Hu Yacai, Ge Jian, Cen Kefa. Pressure drop in a packed bed with sintered ore particles as applied to sinter coolers with a novel vertically arranged design for waste heat recovery [J]. J Zhejiang Univ - Sci 2016;17(2):89–100.
[31] Tian Fuyou, Huang Lianfeng, Fan Liwu, Qian Hongliang, Yu Zitao. Wall effects on the pressure drop in packed beds of irregularly shaped sintered ore particles [J]. Powder Technol 2016;301:1284–93.
[32] Zhou Hao, Lai Zhenya, Lv Laiquan, Fang Hao, Meng Hanxiao, Zhou Mingxi, Cen Kefa. Improvement in the permeability of sintering beds by drying treatment after granulating sinter raw materials containing concentrates [J]. Adv Powder Technol 2020;31:3297–306.
[33] Prasad Likhendra, Muthukumar P. Design and optimization of lab-scale sensible heat storage prototype for solar thermal power plant application [J]. Sol Energy 2013;97:217–29.
[34] Hänchen Markus, Brückner Sarah, Steinfeld Aldo. High-temperature thermal storage using a packed bed of rocks-Heat transfer analysis and experimental validation [J]. Appl Therm Eng 2011;31:1798–806.
[35] Avila-Marin Antonio L, Alvarez-Lara Monica, Fernandez-Reche Jesus. A regenerative heat storage system for central receiver technology working with atmospheric air [J]. Solar PACES 2013, Energy Procedia 2014;49:705–14.
[36] Majumdar Rudrodip, Sandip K, Saha. Computational study of performance of cascaded multi-layered packed-bed thermal energy storage for high temperature applications [J]. J Energy Storage 2020;32:101930.
[37] José Ferná ndez-Seara, Uhıá Francisco J, Jaime Sieres. Experimental analysis of a domestic electric hot water storage tank. Part II: dynamic mode of operation [J]. Appl Therm Eng 2007;27:137–44.
[38] Mawire A, Taole SH. A comparison of experimental thermal stratification parameters for an oil/pebble-bed thermal energy storage (TES) system during charging [J]. Appl Energy 2011;88:4766–78.